

# VARIATIONAL SUBSYNOPTIC ANALYSIS WITH APPLICATIONS TO SEVERE LOCAL STORMS

JOHN M. LEWIS<sup>1</sup>

The University of Oklahoma, Norman, Okla.

## ABSTRACT

Sasaki's variational analysis method is used to describe the subsynoptic surface conditions accompanying severe local storms. Observations are extracted from the network of surface stations that routinely report every hour. The variational analysis filters the observations by constraining the meteorological fields to satisfy a set of governing prognostic equations. The filtering is monotonic and is designed to admit space and time scales of the order of 500 km and 10 hr, respectively.

The analysis is applied to a severe storm situation on June 10, 1968. The development of an intense squall line from the incipient to mature stage is depicted by an index coupling vertical motion and surface moisture. The results demonstrate that dynamically consistent time continuity can be achieved by using the variational method.

## 1. INTRODUCTION

The development and maintenance of severe storms are directly influenced by the physical processes of momentum, heat, and moisture transport in the planetary boundary layer (Sasaki 1966, Bonner 1966, and Sahashi 1968). Sasaki and Lewis (1970) have developed a boundary layer model that is designed to depict the events on a subsynoptic scale (horizontal space scale of the order of 500 km and time scale of the order of 10 hr) accompanying squall-line formation. An objective analysis of surface conditions describing events on this scale and consistent with the governing prognostic equations is vital to both the initialization and forecast. Apart from the necessity of a surface analysis to implement the prediction model, the present study is also motivated by the need for a better understanding of the surface conditions accompanying severe storms.

The dense network of meteorological stations relaying surface information every hour is an excellent source of data for the description of subsynoptic features. In the Midwest, for example, the station spacing is the order of 100 km and, consequently, the description of meteorological distributions with length scales of the order of 500 km is feasible. A strict use of observations, however, will generally admit all those scales detectable by the instrumentation. For the application described above, it is necessary to retain the subsynoptic scale information and remove the short period and wavelength fluctuations (of the order of several minutes and 10 km). This small scale information is considered "noise". Retention of the larger cyclone-scale information should not seriously damage the analysis. That is, the embedded subsynoptic scale features should remain distinct. In principle, the analysis scheme must behave as a low-pass filter.

Hall (1966) and Giles (1967) computed kinematic properties of the surface wind field associated with severe

weather. Both of these investigators used continuous records from the beta-network which is operated by the National Severe Storms Laboratory. They filtered the small-scale information by time averaging the traces for periods ranging from 2 min to 1 hr. Nevertheless, there was a noticeable lack of correlation from one time to the next. Endlich and Mancuso (1968), using conventional hourly data at a fixed time, succeeded in depicting subsynoptic space features on a regular net with a  $1\frac{1}{4}^\circ$  grid interval. Their method fitted a plane locally to the five nearest observations, where more weight was given to observations upstream and downstream than to those along the crosswind direction.

The anisotropic weighting used by Endlich and Mancuso has implicitly accounted for the advection terms in the equations of motion, as proved by Sasaki (1971). Consequently, the time dimension is approximately included in the analysis. Inman (1970) has also demonstrated the advantages of anisotropic weighting in the analysis of the low-level jet and Grayson (1971) has used this type of weighting to advantage in tropical pressure analysis. Time continuity has also been brought into the operational analysis at the National Meteorological Center (NMC) by using the forecast field as a first guess in the successive corrections technique (Cressman 1959). The effect of using the forecast is to indirectly include the prognostic equations in the analysis. This study will use Sasaki's (1969*a*, 1969*b*) variational method because of its ability to directly incorporate the governing dynamical equations into the analysis and thus provide dynamically consistent time continuity.

The variational approach uses a dynamical model to extract information content from the data and reconstruct the meteorological fields that match the model. The model could also be statistical or empirical. Filtering characteristics can be determined from linear analysis and they provide the basis for choosing the weights. The weighting in the analysis scheme is logically tied into the

<sup>1</sup> Present affiliation: Fleet Numerical Weather Central, Naval Postgraduate School, Monterey, Calif.

model and, consequently, has distinct advantages over other objective analysis schemes.

Many parameters and indices have been suggested and used to predict the onset of severe weather activity (U.S. Weather Bureau 1956, Miller 1967). Parameters considered to be important include stability, low-level moisture, and surface convergence. The index,  $q\nabla \cdot \mathbf{V}$ , the product of surface specific humidity and divergence, has proved useful in delineating areas of severe weather activity (Sasaki et al. 1967). This particular parameter and dynamically equivalent forms of it have enjoyed notable success in the parameterization of latent heat release by cumulus convection (e.g., Kuo 1965). Hudson (1970) has demonstrated the applicability of Kuo's parameterization to several middle latitude severe storm situations. His results suggest that well-defined axes of horizontal moisture convergence generally accompany development of strong cumulus convection. Ninomiya (1970), in a study describing the interaction between the mesoscale and synoptic scale, found similar results. This investigation will examine the surface distribution of  $q\nabla \cdot \mathbf{V}$  during the incipient and mature stages of a squall line that formed in the Midwest on June 10, 1968. This distribution will be correlated with radar echoes and surface observations of severe weather.

## 2. GOVERNING EQUATIONS

The meteorological variables are expressed as perturbations about a basic state represented by the U.S. Standard Atmosphere. Since this basic condition assumes a dry atmosphere at rest, the wind and moisture perturbations give the complete description of these variables. The perturbations are nondimensionalized by scaling constants in such a manner that the nondimensional variables are of the order 1. The following notation is used:

$$\begin{aligned} u^* &= V_0 u & \frac{p^*}{\rho} &= f_0 V_0 L_0 \varphi = \varphi_0 \varphi \\ v^* &= V_0 v & x^* &= L_0 x \\ \theta^* &= \theta_0 \theta & y^* &= L_0 y \\ q^* &= q_0 q & z^* &= Z_0 z \\ \rho^* &= \rho_0 \rho & t^* &= \frac{L_0}{V_0} t \\ & & H^* &= H_0 h \end{aligned}$$

where ( )<sup>\*</sup> denotes the dimensional perturbation, ( )<sub>0</sub> indicates the scaling constant, and ( ) the basic state.

The symbols for the nondimensional quantities are

- $x, y$  horizontal Cartesian coordinates on the polar stereographic projection,
- $z$  geometric height above the projection,
- $t$  time,
- $u$   $x$ -component of velocity,
- $v$   $y$ -component of velocity,

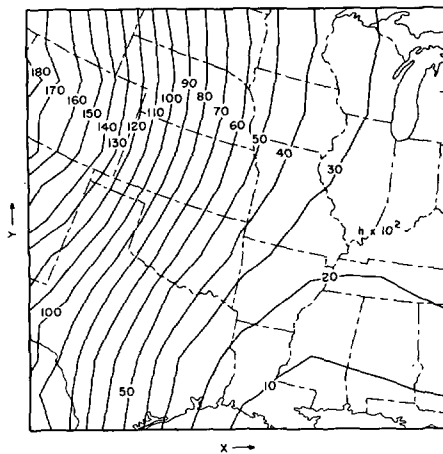


FIGURE 1.—Topographic features over the network in terms of the nondimensional height  $h$ .

$p$  pressure,  
 $\theta$  potential temperature,  
 $\rho$  density,  
 $q$  specific humidity, and  
 $h$  topographic height above mean sea level.

The scaling constants are chosen as follows:

$$\begin{aligned} \theta_0 &= 10^\circ \text{C}, & V_0 &= 10 \text{ m/s}, \\ \rho_0 &= 10^{-1} \text{ kg m}^{-3}, & f_0 &= 10^{-4} \text{ s}^{-1}, \\ q_0 &= 10 \text{ \%}, & L_0 &= 10^6 \text{ m, and} \\ & & Z_0 = H_0 &= 10^3 \text{ m.} \end{aligned}$$

The equations of motion are written in a coordinate system  $(x, y, \sigma, t)$  where

$$\sigma = z - h(x, y). \tag{1}$$

The topographic features are displayed in figure 1. This system is adopted for two reasons: (1) orographic effects appear naturally in the governing equations and (2) the reduction of surface observations to some arbitrary reference level is avoided. The nondimensional equations in the  $x, y, \sigma, t$  system are

$$Ro \dot{u} = v - m \frac{\partial \varphi}{\partial x} + m \frac{\partial h}{\partial x} \frac{\partial \varphi}{\partial \sigma} - \kappa u, \tag{2}$$

$$Ro \dot{v} = -u - m \frac{\partial \varphi}{\partial y} + m \frac{\partial h}{\partial y} \frac{\partial \varphi}{\partial \sigma} - \kappa v, \tag{3}$$

$$\frac{\partial \varphi}{\partial \sigma} = \left( \frac{g Z_0 \theta_0}{f_0 V_0 L_0} \right) \frac{\theta}{\theta_0} = \mu \theta, \tag{4}$$

$$\dot{\theta} = 0, \tag{5}$$

$$\dot{q} = 0, \tag{6}$$

and

$$\varphi = \frac{c^2}{f_0 V_0 L_0} \left( \frac{\rho_0}{\rho} \rho + \frac{\theta_0}{\theta} \theta \right) = \lambda \rho + \beta \theta \tag{7}$$

where

$$(\dot{\quad}) = \left( \frac{\partial}{\partial t} + m u \frac{\partial}{\partial x} + m v \frac{\partial}{\partial y} \right) (\quad),$$

$$m = \frac{1 + \sin 60^\circ}{1 + \sin \phi}, \quad (\text{map scale factor for polar stereographic projection true at } 60^\circ)$$

$\phi$  = latitude,

$$c^2 = \gamma R \bar{T} \quad (\text{speed of sound squared}),$$

and

$$Ro = \frac{V_0}{f_0 L_0} = 10^{-1} \quad (\text{Rossby number}).$$

The derivation of these equations has used the following identities:

$$\frac{\partial}{\partial x} \Big|_z = \frac{\partial}{\partial x} \Big|_\sigma - \frac{\partial h}{\partial x} \frac{\partial}{\partial \sigma},$$

$$\frac{\partial}{\partial y} \Big|_z = \frac{\partial}{\partial y} \Big|_\sigma - \frac{\partial h}{\partial y} \frac{\partial}{\partial \sigma},$$

and

$$\frac{\partial}{\partial z} = \frac{\partial}{\partial \sigma}.$$

The two-dimensionality of the analysis precludes any statement about the conservation of mass. However, incompressibility is tacitly assumed and thus provides a qualitative link between horizontal divergence at the surface and the vertical velocity in the adjoining layer. Equations (2) and (3) are the horizontal momentum equations and eq (4) expresses the hydrostatic balance in terms of the nondimensional perturbations. This form of the hydrostatic equation is derived by substituting from the perturbation form of the equation of state, eq (7), and using the expressions for the distributions of temperature and density in the U.S. Standard Atmosphere. The advective forms of the thermodynamic and moisture equations are represented by eq (5) and (6), respectively.

The frictional force is included in a very approximate way by the Guldberg-Mohn hypothesis (Hess 1959) and appears in the last term of both eq (2) and (3). This specification fails to directly account for the wind shear or thermal stratification and buoyancy effects that are known to contribute to the frictional force. However, it does permit the inclusion of friction in the analysis when observations are available at only one level. The order of magnitude of the parameter  $\kappa$  is found by assuming that the frictional force per unit mass at the surface can be represented by

$$\frac{1}{\rho} \frac{\partial \tau}{\partial z} = C_D \frac{|\partial \mathbf{V}}{\partial z}| \mathbf{V} \quad (9)$$

where  $\tau$  is the horizontal stress vector,  $C_D$  is the drag coefficient, and  $\mathbf{V}$  is the surface wind. This is equivalent to assuming that the stress is proportional to the square of the wind speed (Lettau 1959). Using a value of 1 m/s per 100 m to typify the shear at the ground yields a

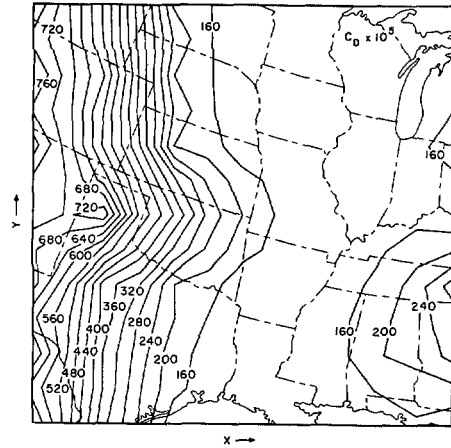


FIGURE 2.—Drag coefficients over the network.

value of  $10^2 C_D$  for  $\kappa$  as it appears in the nondimensional equations. The drag coefficients, as well as topography, are those used at the NMC and discussed by Cressman (1960). The distribution of  $C_D$  is shown in figure 2. With these particular coefficients,  $\kappa$  ranges from 0.1 to 0.8 over the region analyzed.

To incorporate the governing equations into the variational objective analysis, we have written them in finite-difference form. A simple forward-time and centered-space scheme is adopted. Although this scheme is computationally unstable for extended forecasts, it possesses desirable features when used in conjunction with the variational objective analysis (Sasaki 1969b). Specifically, the scheme is algebraically simple and the artificial diffusion associated with more sophisticated schemes such as the Lax-Wendroff (1960) method is reduced. The centered-space scheme is chosen to permit the use of finite difference computational formula germane to manipulations within the framework of the numerical variational method.

The finite difference notation is

$$\nabla_x(\quad) = m \frac{(\quad)_{i+1} - (\quad)_{i-1}}{2\Delta s} \quad (10)$$

and

$$\nabla_y(\quad) = m \frac{(\quad)_{j+1} - (\quad)_{j-1}}{2\Delta s}$$

where  $i$  and  $j$  are indices along the  $x$ - and  $y$ -axes, respectively. The subscripting assumes evaluation at  $i, j$  unless otherwise specified, that is,  $(\quad)_{i+1}$  implies evaluation at  $(\quad)_{i+1, j}$ . For the case study,  $\Delta s = 127$  km and superscripts will be used to denote time levels. Specifically, 0 and 1 will refer to the time for which analysis is desired and a time  $\Delta t$  after analysis time, respectively. For the case study,  $\Delta t = 15$  min.

The finite-difference equations are written as follows:

$$Ro \frac{u^1 - u^0}{\Delta t} = -Ro(u^0 \nabla_x u^0 + v^0 \nabla_y u^0) + v^0 - \nabla_x \rho^0 + (\mu \nabla_x h) \theta^0 - \kappa u^0, \quad (11)$$

$$\text{Ro} \frac{v^1 - v^0}{\Delta t} = -\text{Ro}(u^0 \nabla_x v^0 + v^0 \nabla_y v^0) - u^0 - \nabla_y \varphi^0 + (\mu \nabla_y h) \theta^0 - \kappa v^0, \tag{12}$$

$$\frac{\theta^1 - \theta^0}{\Delta t} = -u^0 \nabla_x \theta^0 - v^0 \nabla_y \theta^0, \tag{13}$$

$$\frac{q^1 - q^0}{\Delta t} = -u^0 \nabla_x q^0 - v^0 \nabla_y q^0, \tag{14}$$

and

$$\varphi^0 = \lambda \rho^0 + \beta \theta^0. \tag{15}$$

### 3. NUMERICAL VARIATIONAL METHOD OF ANALYSIS

This principle of objective analysis was first formulated by Sasaki (1958) and recently extended by him to include a wider class of dynamic constraints (Sasaki 1969a, 1969b, 1970a, 1970b). The variables  $u^1$ ,  $u^0$ ,  $\theta^1$ ,  $\theta^0$ , etc., are required to satisfy the governing dynamics expressed in eq (11)–(15). The analysis is then accomplished by finding those distributions of  $u^0$ ,  $v^0$ ,  $\theta^0$ , and  $q^0$  that minimize the following functional:

$$J = \sum_{i,j} \{ [\tilde{\gamma}(u^0 - \tilde{u})^2 + \tilde{\gamma}(v^0 - \tilde{v})^2 + \tilde{\chi}(q^0 - \tilde{q})^2 + \tilde{\alpha}(\theta^0 - \tilde{\theta})^2 + \tilde{\nu}(\varphi^0 - \tilde{\varphi})^2] + [\gamma_1(u^1 - u^0)^2 + \gamma_1(v^1 - v^0)^2 + \chi_1(q^1 - q^0)^2 + \alpha_1(\theta^1 - \theta^0)^2] + [\eta(\nabla_x u^0 + \nabla_y v^0)^2] \}. \tag{16}$$

The solutions are obtained by requiring the first variation of  $J$  to vanish, that is, the stationary condition for the functional  $J$ . Further conditions on the second variation are unnecessary because of the quadratic nature of  $J$ .

The first set of bracketed terms represent the universal condition for minimizing the variance of the difference between the observed [denoted by ( $\tilde{\quad}$ )] and the analyzed values. The second set of terms incorporates the local rates of change of the variables. These terms give a low-pass filter character to the objective analysis. This feature was discussed by Sasaki (1969b) and will be examined in the appendix.

The amount of divergence, calculated by using centered space-differences for  $u^0$  and  $v^0$ , is controlled by the last term in eq (16) and is called a diagnostic constraint.

The weights  $\alpha_1$ ,  $\tilde{\alpha}$ , etc., ( $>0$ ) are predetermined functions of  $i$ ,  $j$ . Both availability and reliability of observations determine the relative magnitudes of  $\tilde{\alpha}$ ,  $\tilde{\gamma}$ ,  $\tilde{\nu}$ , and  $\tilde{\chi}$ . For example, if the observations of temperature and pressure are more suspect than the wind at a particular grid point, then the ratios  $\tilde{\alpha}/\tilde{\gamma}$  and  $\tilde{\nu}/\tilde{\gamma}$  should be less than 1. Of course, if there are no observations at the grid point, then  $\tilde{\alpha} = \tilde{\gamma} = \tilde{\nu} = \tilde{\chi} = 0$ . The degree of steadiness in the analyzed fields is controlled by  $\gamma_1$ ,  $\chi_1$ , and  $\alpha_1$ . Short waves present in the observations can be filtered by these weights. That is, the amount of damping of short wave components is directly proportional to the magnitudes of  $\gamma_1$ ,  $\chi_1$ , and  $\alpha_1$ . Although these weights imply some damping for the longer wave components,

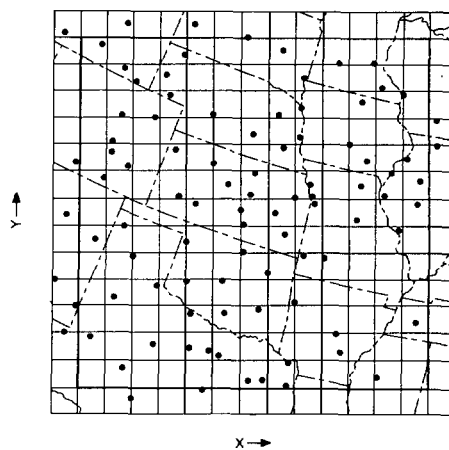


FIGURE 3.—Locations of the surface observation stations used in the objective analysis.

the filter response is monotonically decreasing with increasing wave number and, consequently, produced relatively smaller damping for the long wave components.

Since the observations are invariably collected from irregularly distributed stations, the meaning of  $\tilde{u}$ ,  $\tilde{v}$ , etc., must be clarified. Each observation that is counted at a particular grid point must have an associated observational weight that reflects the precision and accuracy of the data as well as the station-grid point separation. The reliability factors and analytical or statistical weight functions that appear in the successive corrections method (Bergthórsson and Döös 1955, Cressman 1959) are the counterparts to  $\tilde{\alpha}$ ,  $\tilde{\gamma}$ , etc., appearing in the variational formulation. Since the station distribution is very uniform over the analysis region (fig. 3) and there is only one source of information, that is, the hourly reporting stations, the observational weights assume a simple form in this study. Namely, each observation of a particular meteorological variable receives the same weight as any other observation of this same variable provided that they are within 250 km of the grid point.

The particular formulation for the observational weights implicitly smooths the analysis. However, the analysis will still be consistent with the model. Ideally, the position of each observation can be made to coincide with a grid point by taking a fine net. In this case, the variational method will be less ambiguous than other schemes in determining the analysis at grid points where observations are missing. The subsidiary conditions contained in the governing equations or other dynamical constraints can be used to produce an analysis at these points. An initial investigation into this matter has been undertaken by Sasaki (1970c) using data from the National Severe Storms Laboratory network.

The density does not explicitly appear in the functional  $J$ . The analyzed field of density is completely given by the observation and is not determined through the varia-

tional formalism. Again, the term observation is used in accord with the statements in the previous paragraph. For the case study, the data from the surface reporting stations permit only indirect observation of density. That is, the pressure and temperature information are used in conjunction with the equation of state to determine the density.

The variations of  $w^0$ ,  $v^0$ ,  $\theta^0$ , and  $q^0$  vanish on the boundary. This is accomplished by assuming that the analysis at the boundary is identical with the observation. Along with this boundary condition, the following commutative formula is used in the minimization process:

$$\sum_{i,j} \Psi \nabla_x \delta \varphi = - \sum_{i,j} \delta \varphi \nabla_x \Psi \quad (17)$$

where  $\varphi$  and  $\Psi$  are arbitrary functions and  $\delta \varphi$  is assumed to vanish on the boundary. The validity of this commutative formula follows from the symmetric nature of the spatial differencing scheme and has been discussed by Sasaki (1969b).

With the aid of eq (17) and the boundary conditions, the stationary condition can be written:

$$\sum_{i,j} (U \delta u^0 + V \delta v^0 + \Theta \delta \theta^0 + Q \delta q^0) = 0. \quad (18)$$

The minimization is realized only when  $U$ ,  $V$ ,  $\Theta$ , and  $Q$  vanish at each grid point. The expressions for  $U$ ,  $V$ ,  $\Theta$ , and  $Q$  are given as follows:

$$\begin{aligned} U = & -\gamma_1 \Delta t (u^1 - u^0) \nabla_x u^0 + \gamma_1 \Delta t \nabla_x [u^0 (u^1 - u^0)] + \gamma_1 \Delta t \nabla_y [v^0 (u^1 - u^0)] \\ & - \gamma_1 \kappa \frac{\Delta t}{\text{Ro}} (u^1 - u^0) - \gamma_1 \Delta t (v^1 - v^0) \nabla_x v^0 - \gamma_1 \frac{\Delta t}{\text{Ro}} (v^1 - v^0) \\ & - \alpha_1 \Delta t (\theta^1 - \theta^0) \nabla_x \theta^0 - \chi_1 \Delta t (q^1 - q^0) \nabla_x q^0 \\ & + \tilde{\gamma} (u^0 - \tilde{u}) - \eta (\nabla_x^2 u^0 + \nabla_x \nabla_y v^0), \end{aligned} \quad (19)$$

$$\begin{aligned} V = & -\gamma_1 \Delta t (v^1 - v^0) \nabla_y v^0 + \gamma_1 \Delta t \nabla_x [u^0 (v^1 - v^0)] + \gamma_1 \Delta t \nabla_y [v^0 (v^1 - v^0)] \\ & - \gamma_1 \kappa \frac{\Delta t}{\text{Ro}} (v^1 - v^0) - \gamma_1 \Delta t (v^1 - v^0) \nabla_y v^0 + \frac{\gamma_1 \Delta t}{\text{Ro}} (u^1 - u^0) \\ & - \alpha_1 \Delta t (\theta^1 - \theta^0) \nabla_y \theta^0 - \chi_1 \Delta t (q^1 - q^0) \nabla_y q^0 \\ & + \tilde{\gamma} (v^0 - \tilde{v}) - \eta (\nabla_y^2 v^0 + \nabla_x \nabla_y u^0), \end{aligned} \quad (20)$$

$$\begin{aligned} \Theta = & \frac{\gamma_1 \Delta t}{\text{Ro}} \beta \nabla_x (u^1 - u^0) + \left( \frac{\gamma_1 \Delta t}{\text{Ro}} \mu \nabla_x h \right) (u^1 - u^0) \\ & + \frac{\gamma_1 \Delta t}{\text{Ro}} \beta \nabla_y (v^1 - v^0) + \left( \frac{\gamma_1 \Delta t}{\text{Ro}} \mu \nabla_y h \right) (v^1 - v^0) \\ & + \alpha_1 \Delta t \{ \nabla_x [u^0 (\theta^1 - \theta^0)] + \nabla_y [v^0 (\theta^1 - \theta^0)] \} \\ & + \tilde{\alpha} (\theta^0 - \tilde{\theta}) + \beta \tilde{\nu} (\varphi^0 - \tilde{\varphi}), \end{aligned} \quad (21)$$

and

$$Q = \chi_1 \Delta t \{ \nabla_x [u^0 (q^1 - q^0)] + \nabla_y [v^0 (q^1 - q^0)] + \tilde{\chi} (q^0 - \tilde{q}) \}. \quad (22)$$

When the governing prognostic equations, eq (11)-(15), are substituted into eq (19)-(22), the only dependent

variables appearing are  $w^0$ ,  $v^0$ ,  $\theta^0$ , and  $q^0$ . It is also noted that eq (19)-(22) are finite-difference analogs to the second-order nonlinear partial differential equations. The variational analysis problem reduces to the solution of the simultaneous set of equations

$$\begin{aligned} U &= 0 \\ V &= 0 \\ \Theta &= 0 \\ Q &= 0 \end{aligned} \quad (23)$$

at each interior grid point. These are the Euler-Lagrange equations. The network, excluding boundaries, in this study is 14 x 14 and leads to a system of 196 nonlinear algebraic equations in  $w^0$ ,  $v^0$ ,  $\theta^0$ , and  $q^0$ .

The system of equations depicted by eq (23) is solved subject to the rigid boundary conditions that were used to attain the minimization of the functional  $J$ . Sasaki (1970a) has explored the problem of boundary value specification in conjunction with the variational formulation. He used the method of characteristics to investigate the uniqueness of the numerical solution to the Euler-Lagrange equations.

The Gauss-Seidel or successive iteration method is used to find the solution to eq (23) (Isaacson and Keller 1966). The method proceeds from some initial "guess,"  $w^0(1)$ ,  $v^0(1)$ ,  $\theta^0(1)$ ,  $q^0(1)$  by a sequence of successive approximations  $w^0(2)$ ,  $v^0(2)$ ,  $\theta^0(2)$ ,  $q^0(2)$ , etc., which, in principle, converges to the exact solution. The residuals at each grid point  $i, j$  at the  $p$ th stage are denoted by  $R_u(p)$ ,  $R_v(p)$ ,  $R_\theta(p)$ , and  $R_q(p)$ . These residuals are found by substituting the latest approximations into the expressions for  $U$ ,  $V$ ,  $\Theta$ , and  $Q$ , respectively. Reduction of the residuals is achieved by the following formulas:

$$w^0(p+1) = w^0(p) + \alpha_u(p) R_u(p), \quad (24)$$

$$v^0(p+1) = v^0(p) + \alpha_v(p) R_v(p), \quad (25)$$

$$\theta^0(p+1) = \theta^0(p) + \alpha_\theta(p) R_\theta(p), \quad (26)$$

$$q^0(p+1) = q^0(p) + \alpha_q(p) R_q(p), \quad (27)$$

$$\begin{aligned} -\frac{1}{\alpha_u(p)} = -\frac{1}{\alpha_v(p)} = & \gamma_1 \left( \frac{\Delta t}{\text{Ro}} \right)^2 (1 + \kappa^2) + \tilde{\gamma} + 2 \frac{\eta}{(2\Delta s)^2} \\ & + 2\gamma_1 \left( \frac{\Delta t}{2\Delta s} \right)^2 \{ [\overline{u^0(p)}]^2 + [\overline{v^0(p)}]^2 \}, \end{aligned} \quad (28)$$

$$\begin{aligned} -\frac{1}{\alpha_\theta(p)} = & \gamma_1 \left( \frac{\Delta t}{\text{Ro}} \right)^2 \left[ \nabla_x^2 h + \nabla_y^2 h + (\mu \nabla_y h)^2 + \left( \frac{\beta}{\Delta s} \right)^2 \right] \\ & + \tilde{\alpha} + \tilde{\nu} \beta^2 + 2\alpha_1 \left( \frac{\Delta t}{2\Delta s} \right)^2 \{ [\overline{u^0(p)}]^2 + [\overline{v^0(p)}]^2 \}, \end{aligned} \quad (29)$$

and

$$-\frac{1}{\alpha_q(p)} = 2\chi_1 \left( \frac{\Delta t}{2\Delta s} \right)^2 \{ [\overline{u^0(p)}]^2 + [\overline{v^0(p)}]^2 \} + \tilde{\chi}. \quad (30)$$

$\Delta s$  and  $\Delta t$  are the horizontal space and time increments, respectively. The local average values of  $w^0(p)$  and  $v^0(p)$  are denoted by  $\overline{w^0(p)}$  and  $\overline{v^0(p)}$ .

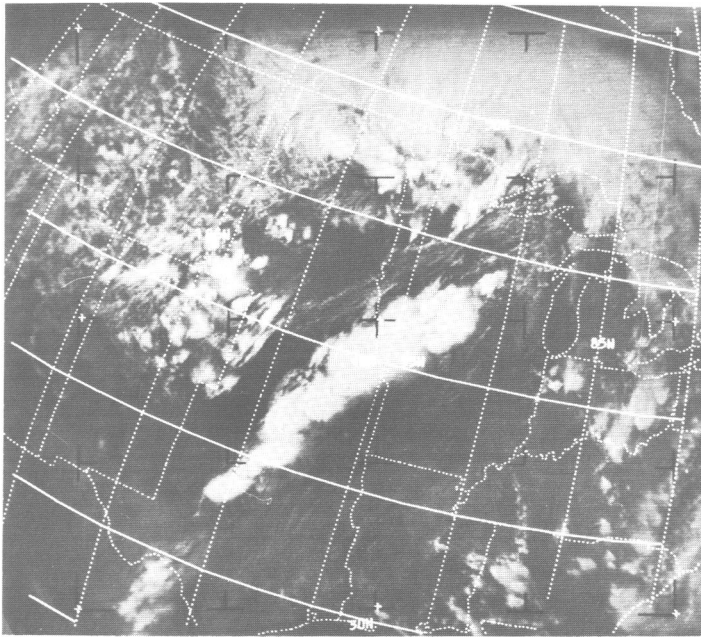


FIGURE 4.—ESSA 5 satellite photograph at 2205 GMT, June 10, 1968, showing the severe storms.

The convergence of a similar set of iteration formulas was fully discussed in the paper by Sasaki and Lewis (1970). The convergence is sensitive to the ratios  $\gamma_1/\tilde{\gamma}$  and  $\alpha_1/\tilde{\alpha}$ . Again, the reader is referred to Sasaki's (1970a) theoretical treatment on both the uniqueness and convergence of the solution obtained by the numerical variational method.

#### 4. APPLICATION TO SQUALL-LINE FORMATION

The case study focuses on development of a squall line in the Midwest on June 10, 1968. The ESSA 5 satellite photograph of the severe storms at 2200 GMT is shown in figure 4. Radar echo was virtually continuous along the band of clouds extending from Texas to Wisconsin and tops ranged from 35,000 to 60,000 ft. A pronounced cyclonic center near 50°N, 95°W is apparent from this photo. The surface cold front extended from the western tip of Lake Superior to southwest Texas skirting the western edge of the squall line. The warm front extended southeastward from Lake Superior toward the southern edge of Lake Huron.

The period of investigation covers the time between the incipient and mature stages of the squall line. For the present study, this span of time is approximately 6 hr. The surface distribution of  $q\nabla \cdot \mathbf{V}$ , the product of the specific humidity and divergence, is examined at hourly intervals between 1700 and 2300 GMT. If the atmosphere is assumed incompressible, this calculation of divergence in the  $x, y, \sigma$  system is explicitly related to  $\dot{\sigma}$ , the material derivative of  $\sigma$ ,

$$\dot{\sigma} = \dot{z} - u^\circ \nabla_x h - v^\circ \nabla_y h \quad (31)$$

and

$$\dot{\sigma}(\xi) = - \int_0^\xi (\nabla_z w^\circ + \nabla_y v^\circ) d\sigma \quad (32)$$

where  $\xi$  is an arbitrary value of the  $\sigma$ -coordinate and  $\dot{\sigma}(0) = 0$  since the normal component of the velocity vanishes at the ground. A negative value of  $\nabla \cdot \mathbf{V}$  (i.e., convergence) at the surface contributes to upward moisture transport. It should be noted, however, that the vanishing of  $\nabla \cdot \mathbf{V}$  could still imply vertical moisture transport due to upslope or downslope motion.

The net of grid points used to analyze the surface conditions is shown in figure 3. The grid length is 127 km, exactly one-third the NMC mesh length. Approximately 130 surface reporting stations were used to obtain observations; their distribution is indicated in figure 3.

The objective analysis was obtained by iteratively solving the equations indicated in eq (23). The weights were as follows:

$$\begin{aligned} \tilde{\gamma} &= 0.1, & \gamma_1 &= 0.1, \\ \tilde{\chi} &= 0.1, & \chi_1 &= 0.1, \\ \tilde{\alpha} &= 0.5, & \alpha_1 &= 1.0, \text{ and} \\ \tilde{\nu} &= 0.5, & \eta &= 0.001. \end{aligned}$$

Relatively small weight was placed on the observed wind because of the poor direction resolution. Observations were to the nearest knot and 10 degrees. A conversion from altimeter setting to station pressure is necessary since only the former quantity is specified in the report. This calculation is made using the distribution of pressure and temperature in the U. S. Standard Atmosphere, and station elevation. With this station pressure and the dew-point observation, the specific humidity is calculated. The ratio of the "dynamics" to observation for the wind, specific humidity, and temperature was chosen of the order of 1. The use of  $\alpha_1/\tilde{\alpha} = 2$  gives slightly more smoothing to the temperature field but is not significantly different from the case where  $\alpha_1/\tilde{\alpha} = 1$ . The weight  $\eta$ , which essentially filters the divergence, is two orders of magnitude smaller than the other weights. Although it would be desirable to choose the weights on a completely physical basis, some care must be exercised, as indicated previously, to ensure convergence of the iterative scheme. The rates of convergence for the set of weights indicated above are shown in figure 5. The cumulative error at each iterative step is indicated by four standard deviations defined as follows:

$$D_u = \sqrt{\frac{\sum_{i=1}^{14} \sum_{j=1}^{14} (R_u)_{i,j}^2}{196}}, \quad (33)$$

$$D_v = \sqrt{\frac{\sum_{i=1}^{14} \sum_{j=1}^{14} (R_v)_{i,j}^2}{196}}, \quad (34)$$

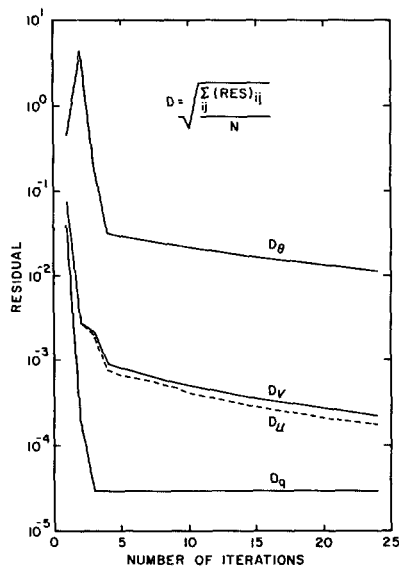


FIGURE 5.—Rate of convergence for eq (19)–(22) in terms of the cumulative residuals. The summation is over  $N$  ( $=196$ ) interior points.

$$D_{\theta} = \sqrt{\frac{\sum_{i=1}^{14} \sum_{j=1}^{14} (R_{\theta})_{i,j}^2}{196}}, \quad (35)$$

$$D_q = \sqrt{\frac{\sum_{i=1}^{14} \sum_{j=1}^{14} (R_q)_{i,j}^2}{196}} \quad (36)$$

where  $R_u$ ,  $R_v$ ,  $R_{\theta}$ , and  $R_q$  are residuals of eq (19)–(22) at each of the 196 interior grid points.

The residuals for each equation show different rates of convergence. Theoretically, the solution is found only when the standard deviations are zero at each grid point. In the present situation, however, the rates of convergence are relatively slow after 20 iterations; in fact, the residual for eq (22) shows no appreciable change after the third iteration.  $D_q$  shows a reduction from  $4 \times 10^{-2}$  to  $3 \times 10^{-5}$  in the 25 iterations. Similarly,  $D_{\theta}$  decreases from  $5 \times 10^{-1}$  to  $10^{-2}$  and the standard deviations  $D_u$  and  $D_v$  drop from  $8 \times 10^{-2}$  to  $2 \times 10^{-4}$ .

The magnitude of the standard deviation is a measure of the cumulative error remaining in the analyzed fields. Part of this error results from using correction factors  $\alpha_u$ ,  $\alpha_v$ ,  $\alpha_{\theta}$ , and  $\alpha_q$ , at each iteration, which are derived by linearizing the Euler-Lagrange equations, eq (19)–(22). Consequently, the reduction of the residuals cannot completely account for the nonlinear terms in eq (19)–(22). The rate of convergence of these equations is shown in figure 5. It is impossible to directly relate the magnitude of the standard deviations to the difference between the exact solution and the solution obtained. Examination of the fields on the last few iterations, however, showed that corrections at a typical grid point were of the order of 0.01 m/s for wind, 0.01°C for temperature, and 0.001 % for specific

humidity. Since the uncertainty in the original measurements is considerably greater than the final corrections, the relaxation process could conceivably be truncated earlier without detriment. The inability to exactly relate error in the meteorological fields to the residuals, however, dictated further iteration.

Figures 6–9 display the areal distribution of  $q\nabla \cdot \mathbf{V}$  along with visual observation and radar echo of cumulus convection and severe weather. The radar information was collected from Amarillo, Tex.; Des Moines, Iowa; Fort Worth, Tex.; Kansas City, Kans.; Oklahoma City, Okla.; and Wichita, Kans. These stations were chosen because of their proximity to the intense squall line discussed previously. Visual observations from the surface network provide a general picture of the severe weather away from the main squall line. The static stability pattern over the network on June 11 at 0000 GMT is shown in figure 10. The stability is represented in terms of an index that is the observed 500-mb temperature minus the temperature of a hypothetical moist parcel that is lifted from the surface to 500 mb. A representative value for the moisture content of the parcel is found by averaging the mixing ratio in the lowest 1000 ft.

The nondimensional form of  $q\nabla \cdot \mathbf{V}$  is depicted in figures 6–9. The dimensional form is obtained by multiplying each number by  $10^{-5} \text{ s}^{-1} \times 10 \text{ \%} \times 10^{-2}$ . Thus, a value of “200” could represent a divergence of  $10^{-5} \text{ s}^{-1}$  and specific humidity of 20 %.

Since  $q$  is positive, the sign immediately indicates convergence (minus) or divergence (plus).

Instead of including the distribution for each hour between 1700 and 2300 GMT, only the alternate hour displays beginning with 1700 GMT are shown. There do not appear to be noticeable gaps or discontinuities that require the hourly interval. The spatial distribution has captured subsynoptic wavelengths of the order of 500 km and effectively removed the shortwave components.

Combination of the  $q\nabla \cdot \mathbf{V}$  patterns and the lifted index patterns essentially couples the parameters most often used by the practical forecaster, namely, low-level moisture, vertical motion, and the stability of the atmosphere. Unfortunately, the lifted index pattern is only available at the end of the period under investigation.

During the incipient stages of development (fig. 6), the northwest corner of the grid has towering cumulus. The radar echoes are scattered and exhibit no correlation with the  $q\nabla \cdot \mathbf{V}$  pattern. The relatively large value,  $-350$ , of  $q\nabla \cdot \mathbf{V}$  near the center of the grid is not associated with convective activity.

As the storms begin to mature, however, the pattern of upward moisture transport used in conjunction with the static instability tends to define the regions of convective activity. The instability pattern must be used with caution, however, since this analysis is valid only at 0000 GMT June 11. The 2100 GMT pattern (fig. 8), which is 4 hr after the initial development, has an

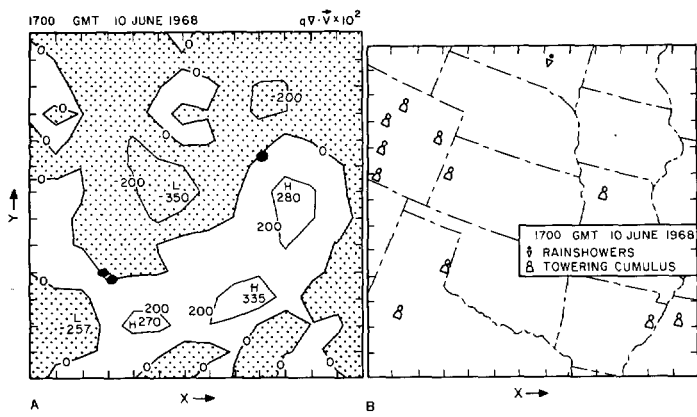


FIGURE 6.—(A) distribution of nondimensional  $q\nabla \cdot \mathbf{V}$  at 1700 GMT June 10. Stippled area represents negative values of  $q\nabla \cdot \mathbf{V}$ ; radar echo patterns are superimposed. (B) surface observations of significant weather at 1700 GMT June 10.

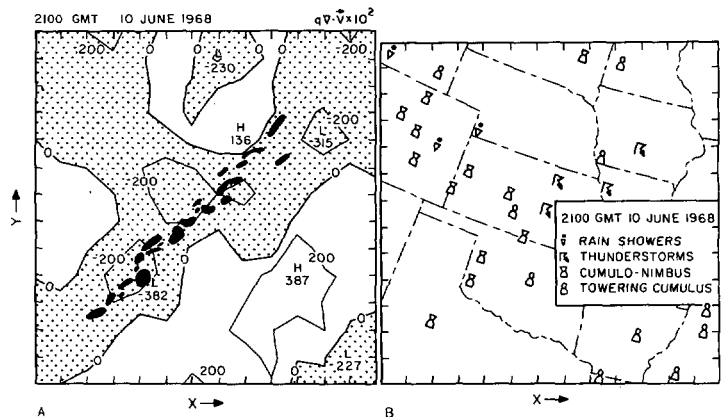


FIGURE 8.—Same as figure 6 except at 2100 GMT.

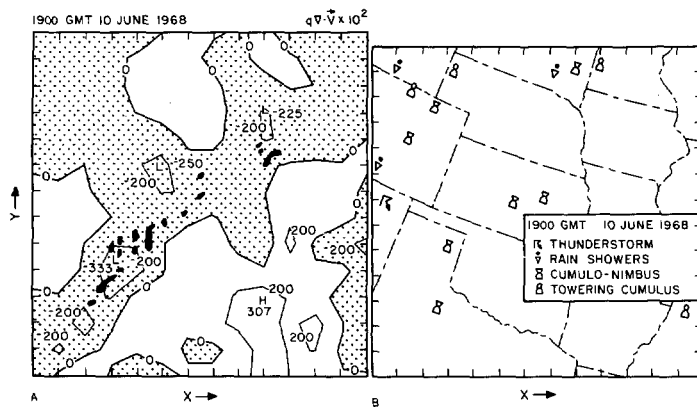


FIGURE 7.—Same as figure 6 except at 1900 GMT.

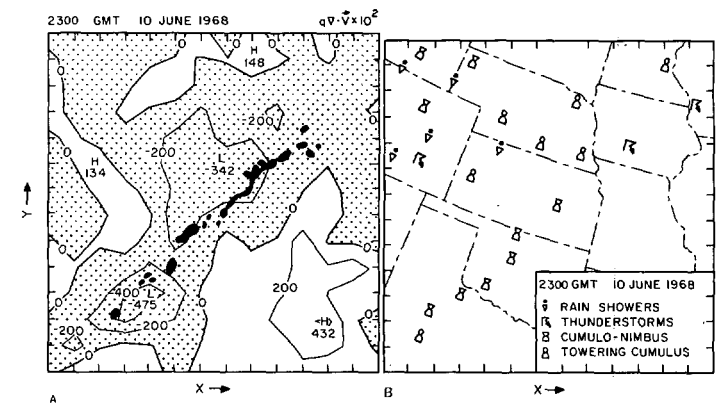


FIGURE 9.—Same as figure 6 except at 2300 GMT.

especially good correlation between convective activity and negative values of  $q\nabla \cdot \mathbf{V}$ . The maximum negative values occur along the squall line and even the scattered activity to the northwest is generally represented by negative values. The stable descending air behind the advancing cold front in Oklahoma and Texas is apparent on the 2100 GMT chart.

There is a noticeable reversal in the sign of  $q\nabla \cdot \mathbf{V}$  over west Texas and New Mexico between 2100 and 2300 GMT. No severe weather was reported in the area during this time span. Further attenuation of such short period oscillations could be accomplished by giving more weight to the second set of terms in eq (16). However, it is difficult to decide, a priori, that these oscillations are irrelevant to severe storms. Consequently, further filtering was considered to be questionable.

### 5. SUMMARY

Although this investigation has been confined to the surface conditions accompanying severe storms, there is

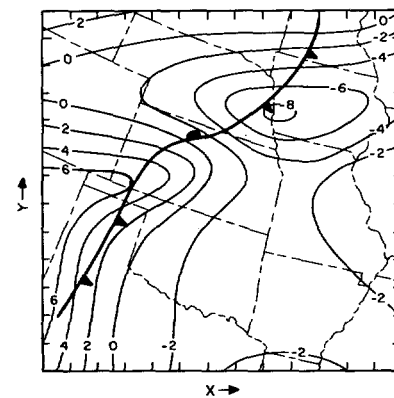


FIGURE 10.—Subjective analysis of the lifted index and of the position of the surface front, at 0000 GMT June 11.

evidence of strong interaction between the subsynoptic and mesoscale motions. Fankhauser (1969) has convincingly shown that this interaction is evident at the middle and upper tropospheric levels also. He obtained good qualitative agreement between the active convective

areas, as shown by radar echo patterns, and the orientation of the strongest kinematic vertical velocities.

The present method has used the "timewise localized variational approach" (Sasaki 1970a). Time continuity has resulted from using the prognostic equations in conjunction with the observations at each particular time level. However, the derived Euler-Lagrange equations do not have any local change terms. Future work is aimed at incorporating observations at the various time levels explicitly into the analysis at a particular time. Such an option is available within the framework of the variational technique and has been demonstrated by application to gust-front analysis in the National Severe Storms Laboratory mesonet network of surface stations (Sasaki 1970c).

**APPENDIX—FILTERING PROPERTIES OF THE ANALYSIS SCHEME**

Some features of the filtering implied by this analysis scheme are examined. A simpler set of dynamic equations is employed so that the algebraic manipulations can be significantly reduced. These equations are

$$u^1 - u^0 = -u^0 \Delta t \nabla_x u^0 - \frac{\Delta t}{Ro} \nabla_x \phi^0 \tag{37}$$

$$\theta^1 - \theta^0 = -u^0 \Delta t \nabla_x \theta^0 \tag{38}$$

where all variables are nondimensionalized in accord with the text.

The functional to be minimized is

$$I = \sum_i [\gamma_1 (u^1 - u^0)^2 + \alpha_1 (\theta^1 - \theta^0)^2 + \tilde{\gamma} (u^0 - \tilde{u})^2 + \tilde{\alpha} (\theta^0 - \tilde{\theta})^2 + \tilde{\nu} (\phi^0 - \tilde{\phi})^2] \tag{39}$$

The Euler-Lagrange equations are linearized to make the system mathematically tractable. This, however, does limit the analysis since the temperature is uncoupled from the pressure and wind. The linearized system is

$$\gamma_1 (U \Delta t)^2 \nabla_x^2 u^0 + \gamma_1 \frac{U(\Delta t)^2}{Ro} \nabla_x^2 \phi^0 - \tilde{\gamma} (u^0 - \tilde{u}) = 0, \tag{40}$$

$$\gamma_1 \frac{U(\Delta t)^2}{Ro} \nabla_x^2 u^0 + \gamma_1 \left(\frac{\Delta t}{Ro}\right)^2 \nabla_x^2 \phi^0 - \tilde{\nu} (\phi^0 - \tilde{\phi}) = 0, \tag{41}$$

and

$$\alpha_1 (U \Delta t)^2 \nabla_x^2 \theta^0 - \tilde{\alpha} (\theta^0 - \tilde{\theta}) = 0 \tag{42}$$

where  $U$  is a constant (mean) velocity.

The continuous distributions of wind, pressure, and temperature observations are given by

$$\tilde{u} = \tilde{A} e^{ikx},$$

$$\tilde{\phi} = \tilde{B} e^{ikx},$$

and

$$\tilde{\theta} = \tilde{C} e^{ikx} \tag{43}$$

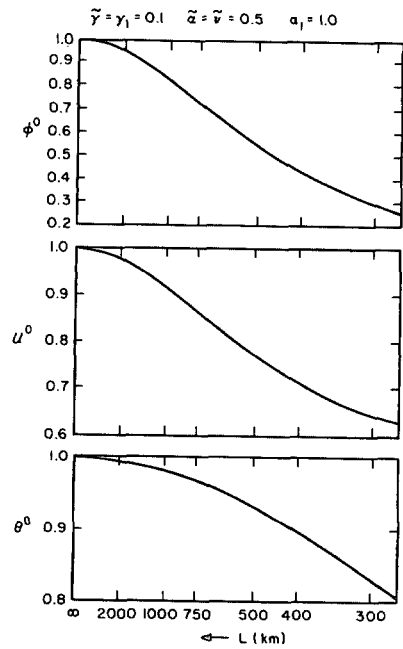


FIGURE 11.—Low-pass filter characteristics of the numerical variational method.

where  $k$  is the wave number ( $=2\pi/L$ ), and, for the purposes of this analysis, we assume  $\Delta s \rightarrow 0$  so that the difference operators become differential operators. The solution of eq (40)–(42) is

$$A = \frac{-\tilde{\nu} \left[ 1 + \frac{\gamma_1}{\tilde{\nu}} \left( \frac{\Omega}{URo} \right)^2 \right] \tilde{\gamma} \tilde{A} + \gamma_1 \frac{\Omega^2}{URo} \tilde{\nu} \tilde{B}}{\left( \gamma_1 \frac{\Omega^2}{URo} \right)^2 - \tilde{\gamma} \tilde{\nu} \left[ 1 + \frac{\gamma_1}{\tilde{\nu}} \Omega^2 \right] \left[ 1 + \frac{\gamma_1}{\tilde{\nu}} \left( \frac{\Omega}{URo} \right)^2 \right]}, \tag{44}$$

$$B = \frac{\tilde{\gamma} \left( 1 + \frac{\gamma_1}{\tilde{\nu}} \Omega^2 \right) \tilde{\nu} \tilde{B} - \gamma_1 \frac{\Omega^2}{URo} \tilde{\gamma} \tilde{A}}{\tilde{\gamma} \tilde{\nu} \left[ 1 + \frac{\gamma_1}{\tilde{\nu}} \Omega^2 \right] \left[ 1 + \frac{\gamma_1}{\tilde{\nu}} \left( \frac{\Omega}{URo} \right)^2 \right] - \left( \gamma_1 \frac{\Omega^2}{URo} \right)^2}, \tag{45}$$

and

$$C = \frac{\tilde{C}}{1 + \frac{\alpha_1}{\tilde{\alpha}} \Omega^2} \tag{46}$$

where  $\Omega = kU\Delta t$  and  $A$ ,  $B$ , and  $C$  are the Fourier coefficients of wave number  $k$  for  $u^0$ ,  $\phi^0$ , and  $\theta^0$ , respectively.

The solutions are calculated for the particular values of  $\tilde{\gamma}$ ,  $\tilde{\alpha}$ ,  $\tilde{\nu}$ ,  $\gamma_1$ , and  $\alpha_1$  used for the case study. These results are shown in figure 11. The low-pass filter character is displayed in all three distributions with noticeably more short wavelength damping in the pressure field than in either the wind or temperature field.

**ACKNOWLEDGMENTS**

Professor Sasaki has provided guidance throughout the course of this research effort. Thanks are due both Dr. Inman and

Prof. Sasaki for critically reading the manuscript and Mr. Jess Charba, who willingly assisted in the analysis of the lifted index.

The staff of the Computing Facility at the National Center for Atmospheric Research (NCAR), which is sponsored by the National Science Foundation, have been most cooperative. The calculations were performed on NCAR's Control Data Corporation 6600 computer. The work was performed under ESSA Contract No. E22-43-70(G).

#### REFERENCES

- Bergthórsson, Páll, and Döös, Bo R., "Numerical Weather Map Analysis," *Tellus*, Vol. 7, No. 3, Stockholm, Sweden, Aug. 1955, pp. 329-340.
- Bonner, William D., "Case Study of Thunderstorm Activity in Relation to the Low-Level Jet," *Monthly Weather Review*, Vol. 94, No. 3, Mar. 1966, pp. 167-178.
- Cressman, George P., "An Operational Objective Analysis System," *Monthly Weather Review*, Vol. 87, No. 10, Oct. 1959, pp. 367-374.
- Cressman, George P., "Improved Terrain Effects in Barotropic Forecasts," *Monthly Weather Review*, Vol. 88, Nos. 9-12, Sept.-Dec. 1960, pp. 327-342.
- Endlich, R. M., and Mancuso, R. L., "Objective Analysis of Environmental Conditions Associated With Severe Thunderstorms and Tornadoes," *Monthly Weather Review*, Vol. 96, No. 6, June 1968, pp. 342-350.
- Fankhauser, James C., "Convective Processes Resolved by a Mesoscale Rawinsonde Network," *Journal of Applied Meteorology*, Vol. 8, No. 5, Oct. 1969, pp. 778-798.
- Giles, J. D., "An Investigation of the Mesoscale Pattern Associated With Severe Storms," M.S. thesis, Department of Meteorology, University of Oklahoma, Norman, 1967, 48 pp.
- Grayson, T., "Global Band Surface Analysis of Pressure and Wind Including the Tropics," *Fleet Numerical Weather Central Technical Memorandum*, Naval Postgraduate School, Monterey, Calif., 1971, 35 pp.
- Hall, S. J., "Patterns of Certain Kinematic Properties of Squall Lines Related to Their Radar Echoes," *Oklahoma University Research Institute Technical Report*, 1966, 25 pp.
- Hess, Seymour L., *Introduction to Theoretical Meteorology*, Henry Holt and Co., New York, N.Y., 1959, 362 pp. (see p. 179).
- Hudson, Horace R., "On the Relationship Between Horizontal Moisture Convergence and Convective Cloud Formation," *ESSA Technical Memorandum ERLTM-NSSL 45*, National Severe Storms Laboratory, Norman, Okla., Mar. 1970, 29 pp.
- Inman, Rex L., "Papers on Operational Objective Analysis Schemes at the National Severe Storms Forecast Center," *NOAA Technical Memorandum ERLTM-NSSL 51*, National Severe Storms Laboratory, Norman, Okla., Nov. 1970, 91 pp.
- Isaacson, Eugene, and Keller, Herbert Bishop, *Analysis of Numerical Methods*, John Wiley and Sons, Inc., New York, N.Y., 1966, 556 pp.
- Kuo, H.-L., "On Formation and Intensification of Tropical Cyclones Through Latent Heat Released by Cumulus Convection," *Journal of the Atmospheric Sciences*, Vol. 22, No. 1, Jan. 1965, pp. 40-63.
- Lax Peter D., and Wendroff, Burton, "Systems of Conservation Laws," *Communications on Pure and Applied Mathematics*, Vol. 13, Interscience Publications, Inc., New York, N.Y., 1960, pp. 217-237.
- Lettau, Heinz H., "Wind Profile, Surface Stress and Geostrophic Drag Coefficients in the Atmospheric Surface Layers," *Advances in Geophysics*, Vol. 6, Academic Press, New York, N.Y., 1959, pp. 241-257.
- Miller, Robert C., "Notes on Analysis and Severe-Storm Forecasting Procedures of the Military Weather Warning Center," *U.S. Air Weather Service Technical Report No. 200*, Kansas City, Mo., July 1967, 125 pp.
- Ninomiya, Kozo, "Dynamical Aspects of the Development of Mesoscale Convective Storms," Paper presented at the American Meteorological Society Conference on Motion and Dynamics of the Atmosphere, Houston, Texas, Mar. 23-25, 1970.
- Sahashi, Ken, "Measurements of Wind and Temperature From WKY-TV Tower, Oklahoma City, in Conjunction With Severe Storms," Paper presented at the National Severe Storms Laboratory (NSSL) Seminar, Norman, Okla., June 1968.
- Sasaki, Yoshikazu, "An Objective Analysis Based on the Variational Method," *Journal of the Meteorological Society of Japan*, Vol. 36, No. 3, Tokyo, June 1958, pp. 77-88.
- Sasaki, Yoshikazu, "Structure and Motion of Convective Systems Under Influences of Boundary Layer," *Oklahoma University Atmospheric Research Institute Technical Report No. ARL-1523-1*, Grant Nos. WBG-72 and NSF-GS-238, Norman, 1966, 23 pp.
- Sasaki, Yoshikazu, "Numerical Variational Method of Analysis and Prediction," *Proceedings of the WMO/IUGG Symposium on Numerical Weather Prediction, Tokyo, Japan, November 26-December 4, 1968*, Japan Meteorological Agency, Tokyo, Mar. 1969a, pp. VII-25-VII-33.
- Sasaki, Yoshikazu, "Proposed Inclusion of Time Variation Terms, Observational and Theoretical, in Numerical Variational Objective Analysis," *Journal of the Meteorological Society of Japan*, Vol. 47, No. 2, Tokyo, Apr. 1969b, pp. 115-124.
- Sasaki, Yoshikazu, "Some Basic Formalisms in Numerical Variational Analysis," *Monthly Weather Review*, Vol. 98, No. 12, Dec. 1970a, pp. 875-883.
- Sasaki, Yoshikazu, "Numerical Variational Analysis Formulated Under the Constraints as Determined by Longwave Equations and a Low-Pass Filter," *Monthly Weather Review*, Vol. 98, No. 12, Dec. 1970b, pp. 884-898.
- Sasaki, Yoshikazu, "Numerical Variational Analysis With Weak Constraint and Application to Surface Analysis of Severe Storm Gust," *Monthly Weather Review*, Vol. 98, No. 12, Dec. 1970c, pp. 899-910.
- Sasaki, Yoshikazu, "A Theoretical Interpretation of Anisotropically Weighted Smoothing on the Basis of Numerical Variational Analysis," *Monthly Weather Review*, Vol. 99, No. 9, Sept. 1971, pp. 698-707.
- Sasaki, Yoshikazu, and Lewis, John M., "Numerical Variational Objective Analysis of the Planetary Boundary Layer in Conjunction With Squall Line Formation," *Journal of the Meteorological Society of Japan*, Ser. 2, Vol. 48, No. 5, Tokyo, Oct. 1970, pp. 381-399.
- Sasaki, Yoshikazu, Lewis, John M., Chen, T. S., French, L., and Harmon, J., "Dynamical Forecasting of Severe Local Storms," *University of Oklahoma Research Institute Technical Report*, 1967, 20 pp.
- U.S. Weather Bureau, "Forecasting Tornadoes and Severe Thunderstorms," *Forecasting Guide No. 1*, Washington, D.C., 1956, 35 pp.

[Received October 8, 1970; revised January 20, 1971]